This is the accepted manuscript made available via CHORUS. The article has been published as:

Spin Seebeck effect in the layered ferromagnetic insulators CrSiTe_{3} and CrGeTe_{3}

Naohiro Ito, Takashi Kikkawa, Joseph Barker, Daichi Hirobe, Yuki Shiomi, and Eiji Saitoh

Phys. Rev. B **100**, 060402 — Published 5 August 2019

DOI: 10.1103/PhysRevB.100.060402

Spin Seebeck Effect in Layered Ferromagnetic Insulators $CrSiTe_3$ and $CrGeTe_3$

Naohiro Ito,[1,*] Takashi Kikkawa,[1,2] Joseph Barker,[1,3]

Daichi Hirobe,[1,†] Yuki Shiomi,[4] and Eiji Saitoh[1,2,5,6,7]

[1]*Institute for Materials Research, Tohoku University, Sendai 980-8577, Japan*

[2]*WPI Advanced Institute for Materials Research,*

Tohoku University, Sendai 980-8577, Japan

[3]*School of Physics and Astronomy,*

University of Leeds, Leeds, LS2 9JT, UK

[4]*Department of Basic Science, The University of Tokyo, Tokyo 153-8902, Japan*

[5]*Department of Applied Physics, The University of Tokyo, Tokyo 113-8656, Japan*

[6]*Center for Spintronics Research Network,*

Tohoku University, Sendai 980-8577, Japan

[7]*Advanced Science Research Center,*

Japan Atomic Energy Agency, Tokai 319-1195, Japan

(Dated: July 17, 2019)

Abstract

We have studied the longitudinal spin Seebeck effect (LSSE) in the layered ferromagnetic insulators $CrSiTe_3$ and $CrGeTe_3$ covered by Pt films in the measurement configuration where spin current traverses the ferromagnetic Cr layers. The LSSE response is clearly observed in the ferromagnetic phase and—in contrast to a standard LSSE magnet $Y_3Fe_5O_{12}$—persists above the critical temperatures in both $CrSiTe_3$/Pt and $CrGeTe_3$/Pt samples. With the help of a numerical calculation, we attribute the LSSE signals observed in the paramagnetic regime to exchange-dominated interlayer transport of in-plane paramagnetic moments reinforced by short-range ferromagnetic correlations and strong Zeeman effects.

The longitudinal spin Seebeck effect (LSSE) generates spin currents in magnetic materials when a temperature gradient is applied [1]. By injecting this spin current into a paramagnetic metal it can be measured as a voltage through the inverse spin Hall effect. Because of the simple bilayer structure needed to generate a thermoelectric voltage, LSSE devices have a potential use as thermoelectric conversion elements [2, 3]. From the point of basic physics, the LSSE is sensitive to spin correlations [4, 5], and thus can be exploited as a probe to study the dynamical spin susceptibility in magnetic materials [6, 7]. The LSSE was originally found in ferro(ferri)magnets and later measured also in antiferromagnets [8–11] and paramagnets [12, 13]. However, the LSSE has not been studied in magnetic materials with two-dimensional (2D) crystal structures, even though 2D materials—such as transition-metal chalcogenides—have drawn extensive research attention due to their extraordinary magnetic properties [14].

The layered ferromagnetic insulators $CrSiTe_3$ and $CrGeTe_3$ have been studied recently due to their intriguing physical properties. First-principle calculations [15, 16] predicted that the ferromagnetism in $CrSiTe_3$ survives even down to a monolayer thickness and indeed ferromagnetism in bilayer flakes of $CrGeTe_3$ was experimentally confirmed [17]. The Cr layers possess a graphene-like honeycomb structure and exotic properties are expected to arise in hetero-structures fabricated with related 2D materials by van der Waals epitaxy. Furthermore, it has been reported that $CrGeTe_3$ acts as an ideal ferromagnetic substrate for the growth of the popular topological insulator Bi_2Te_3 [18].

In this paper, we studied the LSSE [1] in the ferromagnets $CrSiTe_3$ and $CrGeTe_3$ in contact with Pt films. The crystal structure of $CrSiTe_3$ and $CrGeTe_3$ is illustrated schematically

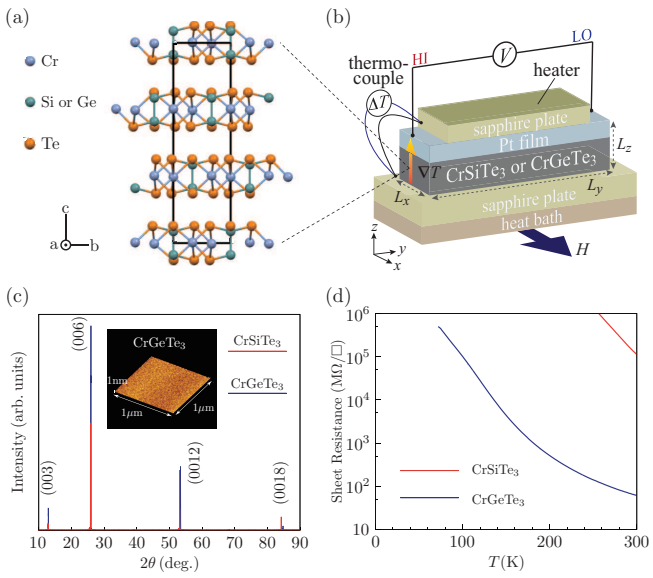

FIG. 1: (a) Schematic illustration of the crystal structure of $CrSiTe_3$ and $CrGeTe_3$. (b) Schematic illustration of the LSSE measurements. H denotes the external magnetic field and ΔT (∇T) the temperature difference (gradient). (c) X-ray diffraction patterns of $CrSiTe_3$ and $CrGeTe_3$ single crystals. The inset is an atomic force microscope image of the surface of $CrGeTe_3$. (d) T dependence of the sheet resistance for $CrSiTe_3$ and $CrGeTe_3$.

in Fig. 1(a). The Cr^{3+} (Spin 3/2) ions form a honeycomb lattice in the *ab*-plane with the Si or Ge atoms in the center of the hexagon and the Cr^{3+} atoms are surrounded by octahedra of Te atoms [19–21]. The honeycomb layers stack along the *c*-axis, held together by van der Waals interactions, forming a quasi-2D structure with a highly anisotropic magnetic environment. Interestingly, it was reported that $CrSiTe_3$—with a Curie temperature of $T_C \approx 31$ K—has short-range, in-plane ferromagnetic correlations which survive up to at least 300 K, whereas out-of-plane correlations disappear above 50 K [22]. This is because the in-plane exchange coupling is more than five times greater than the out-of-plane coupling [22].

Single crystals of $CrSiTe_3$ and $CrGeTe_3$ were grown by a self-flux method, following the procedure described in the literature [18, 23, 24]. First, high purity powders of Cr, Si, Ge, and Te were placed in alumina crucibles in a molar ratio of Cr:Si:Te = 1:2:6 and Cr:Ge:Te

= 1:3:18; the excess Si, Ge and Te work as a flux for the crystal growth. The alumina crucibles were placed inside quartz tubes and sealed under argon atmosphere (pressure of 0.3 bar). The ampoules were then heated up to 1150 °C (700 °C), and maintained at theses temperatures for 16 hours (22 days) and then slowly cooled to 700 °C (500 °C) for $CrSiTe_3$ ($CrGeTe_3$), followed by centrifugation to remove excess flux. Single crystals were obtained as plate-like forms with the size of several millimeters.

The sample structures were characterized by X-ray diffraction with Cu-Kα1 radiation at room temperature. Figure 1(c) shows X-ray diffraction patterns of the $CrSiTe_3$ and $CrGeTe_3$ samples. Both samples show only sharp $(00n)$ peaks; no impurity peaks were observed. The widest planes of the single crystals were determined as crystallographic ab-planes. The lattice parameter was estimated to be $c = 20.67$ Å for $CrSiTe_3$ and $c = 20.56$ Å for $CrGeTe_3$, consistent with previous reports [19, 21, 23, 25, 26].

The temperature (T) dependence of the in-plane sheet resistance of $CrSiTe_3$ and $CrGeTe_3$ crystals are shown in Fig. 1(d). For $CrSiTe_3$, the sheet resistance increases with decreasing T, and goes beyond the measurement limit around 250 K; at lower temperatures, the $CrSiTe_3$ samples can be viewed as a good insulator. The sheet resistance of $CrGeTe_3$ shows a similar T dependence, but is three orders of magnitude smaller than that of $CrSiTe_3$. In $CrGeTe_3$/Pt devices ferromagnetic itinerant transport, such as the anomalous Nernst effect [27], is expected to be negligible below ≈ 100 K.

Magnetic properties were measured with a vibrating sample magnetometer. Figure 2(a) shows the magnetization M versus magnetic field H applied in the ab-plane of $CrSiTe_3$ and $CrGeTe_3$ crystals at $T = 5$ K. A magnetization curve with a saturation magnetization

of about 2.7 μ_B was observed for both samples—in good agreement with the spin 3/2 of Cr^{3+} ions. In Fig. 2(b), we show the T dependence of M for $CrSiTe_3$ and $CrGeTe_3$ at $H = 1$ kOe. A sharp paramagnetic to ferromagnetic phase transition was observed in both samples [23, 26].

We evaluated the critical temperature T_C for $CrSiTe_3$ and $CrGeTe_3$ using a modified Arrott plot analysis [26, 28, 29]. This method determines the critical exponents β and γ by the fitting of H/M and M with the Arrott-Noaks equation:

$$\left(\frac{H}{M}\right)^{1/\gamma} = a\frac{T - T_C}{T} + bM^{1/\beta} \tag{1}$$

where a and b are fitting parameters. Fitting of Eq. (1) with a rigorous iterative method [26, 28, 29] gives $T_C = 31.3$ K for $CrSiTe_3$ and $T_C = 64.7$ K for $CrGeTe_3$ [see Figs. 2(c) and 2(d), where the estimated critical exponents β and γ are also shown]. The values of β are smaller than in three-dimensional (3D) spin models ($\beta_{\text{3D Heisenberg}} = 0.365$ and $\beta_{\text{3D Ising}} = 0.325$) but larger than 2D spin models ($\beta_{\text{2D Ising}} = 0.125$), signalling a 2D character of the ferromagnetic transition [26, 28].

To measure the LSSE we used samples of $CrSiTe_3$ ($CrGeTe_3$) with dimensions $L_x =$ 1.5 mm (0.8 mm), $L_y = 3.5$ mm (4.4 mm), and $L_z = 0.2$ mm (75 μm) and deposited a 5-nm-thick Pt film on the surface [see Fig. 1(b)]. To ensure clean and flat interfaces, their (as-grown) top (ab-plane) surfaces were exfoliated using adhesive tape before the Pt deposition; the resultant surface roughness (R_a) of the $CrSiTe_3$ and $CrGeTe_3$ samples were 5.4×10^{-2} nm and 4.1×10^{-2} nm, respectively confirming the samples are very flat and smooth [see the atomic force microscope image for the $CrGeTe_3$ surface shown in the inset

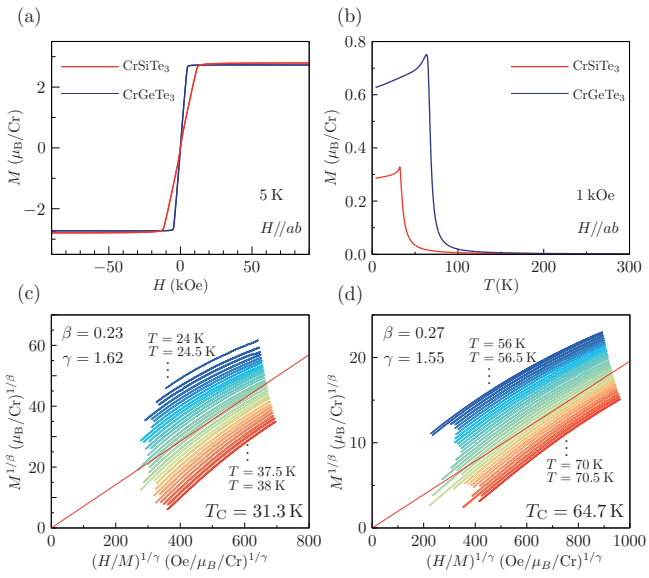

FIG. 2: (a) H dependence of M (M-H curve) for $CrSiTe_3$ and $CrGeTe_3$ at 5 K. (b) T dependence of M for $CrSiTe_3$ and $CrGeTe_3$ at 1 kOe (below saturation). (c),(d) Modified Arrott plot of isotherms for (c) $CrSiTe_3$ and (d) $CrGeTe_3$, from which the T_C values are determined. The red straight lines in (c) and (d) are eq.(1) at $T = T_C$.

to Fig. 1(c)]. To apply a temperature gradient, ∇T, along the c-axis [z-axis in Fig. 1(b)] of the samples, the $CrSiTe_3$/Pt and $CrGeTe_3$/Pt were sandwiched between two sapphire plates; a 100 Ω chip resistor was fixed on one plate, while the other is connected to a heat bath [see Fig. 1(b)]. By applying a charge current to the resistor, a constant temperature difference, ΔT, of 2 K (1 K) was generated for the $CrSiTe_3$/Pt ($CrGeTe_3$/Pt) sample that was measured by using type-E thermocouples attached to the two sapphire plates [see Fig. 1(b)]. The external magnetic field H was applied in the ab-plane (along the x-axis) and the thermal voltage V between the ends of the Pt film (along the y-axis; its distance L_y) was measured. We define the LSSE voltage $V_{\rm LSSE}$ as the antisymmetric contribution of the thermoelectric voltage: $[V(+H) - V(-H)]/2$. Hereafter, we mainly use the transverse thermopower $S = (V_{\rm LSSE}/\Delta T)(L_z/L_y)$ as the normalized LSSE voltage.

Figures 3(a) and 3(c) show the H dependence of S in the $CrSiTe_3$/Pt and $CrGeTe_3$/Pt

samples at selected temperatures. In the ferromagnetic phase below T_C clear LSSE signals were observed for both the samples [see the dark- and bright-blue solid lines in Figs. 3(a) and 3(c)]. The S-H curves for the $CrSiTe_3$/Pt and $CrGeTe_3$/Pt qualitatively agree with the M-H curves for the bulk $CrSiTe_3$ and $CrGeTe_3$ crystals as shown in Figs. 3(b) and 3(d); by increasing H from zero, the S amplitude rapidly increases and almost saturates above the magnetization saturation field H_c for M ($\sim$ 15 kOe for $CrSiTe_3$ and $\sim$ 6 kOe for $CrGeTe_3$). This is a characteristic feature of the LSSE [3].

Interestingly, clear LSSE signals are observed at the paramagnetic phases above T_C where long-range ferromagnetic ordering is absent. The red solid lines in Figs. 3(a) and 3(c) represent the S-H curves for the $CrSiTe_3$/Pt and $CrGeTe_3$/Pt samples at 35 K and 70 K, higher than their T_C values of 31.3 K and 64.7 K, respectively. We attribute the non-linear H dependence of S to the LSSE as the observed S signals should originate purely from the LSSE in the paramagnetic phase since the Nernst effect in $CrSiTe_3$ and $CrGeTe_3$ will be vanishingly small for the high resistivities at these temperatures.

We systematically measured the T dependence of the LSSE. The dark-blue plots in Figs. 4(a) and 4(c) show the S versus T results for the $CrSiTe_3$/Pt and $CrGeTe_3$/Pt samples, at a low field of H = 15 kOe and 6 kOe, respectively. By increasing T from low temperature, S increases and takes a maximum value at around 15 K (30 K) for the $CrSiTe_3$/Pt ($CrGeTe_3$/Pt) sample. Further increasing T, S decreases. The behavior is similar to the LSSE in a 3D ferro(ferri)magnet $Y_3Fe_5O_{12}$ (YIG) [30–32]. In contrast to the YIG case however, the S signal persists at and above T_C [see the dark-blue plots around dashed lines in Figs. 4(a) and 4(c)]. Upon further increasing T the LSSE signal disappears around 50 K

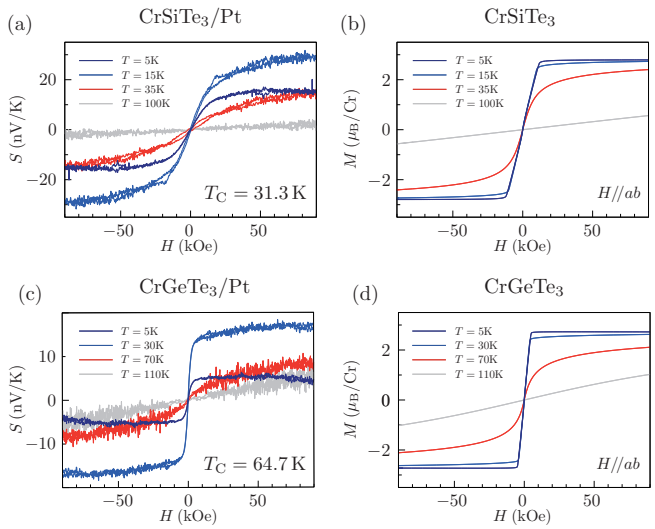

FIG. 3: H dependence of the normalized LSSE signal S in (a) $CrSiTe_3$/Pt and (c) $CrGeTe_3$/Pt and H dependence of M for (b) $CrSiTe_3$ and (d) $CrGeTe_3$ at several temperatures, where H was applied in the ab-plane and swept between ± 90 kOe.

(90 K) for the $CrSiTe_3$/Pt ($CrGeTe_3$/Pt) sample, which is higher than T_C by ~ 20 K.

The observation of the LSSE in the paramagnetic phase above T_C gives an insight into the different roles of the anisotropic (in-plane and out-of-plane) spin correlations in LSSE. The quasi-2D ferromagnetism of $CrSiTe_3$ and $CrGeTe_3$ is due to the significant difference in strength of the in-plane and out-of-plane exchange interactions [17, 22]. In $CrSiTe_3$ the in-plane exchange coupling strength $J_{ab} \sim 15$ K is more than five times larger than the out-of-plane J_c [22]. Short-range in-plane ferromagnetic correlations even persist to room temperature, while the out-of-plane correlations rapidly diminish above T_C [22]. If the LSSE we measured was driven by spin pumping from the in-plane ($\perp \nabla T$) spin correlations adjacent to the Pt interface, the LSSE signal would appear until 300 K. That is not the case [Fig. 5(a)]. Our experimental results show the vital role of spin transport between the planes (along the temperature gradient - $\parallel \nabla T$) to create the non-equilibrium magnon population essential for the appearance of LSSE [Fig. 5(b)] [33, 34]. This experimentally decouples the

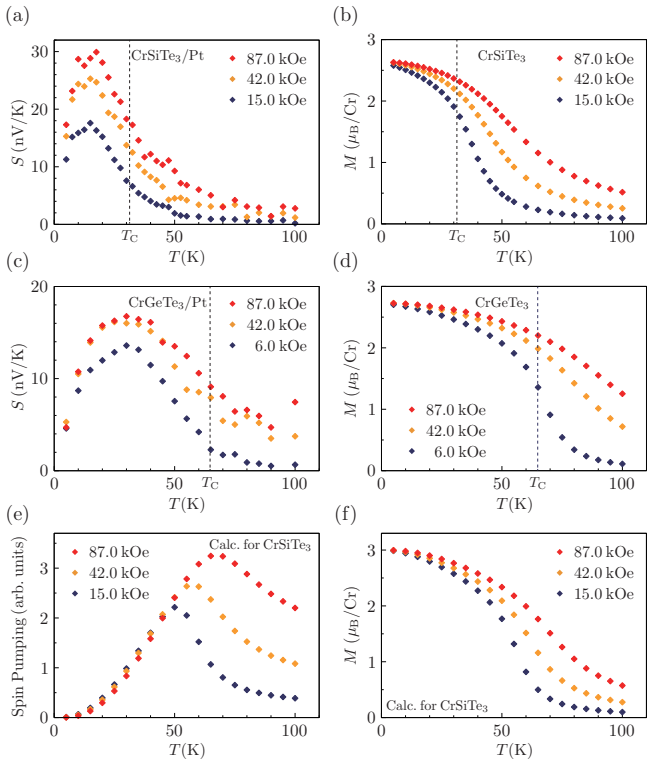

FIG. 4: T dependence of the normalized LSSE signal S (a) at 15.0, 42.0, and 87.0 kOe in $CrSiTe_3$/Pt and (c) at 6.0, 42.0, and 87.0 kOe in $CrGeTe_3$/Pt. T dependence of the magnetization M (a) at 15.0, 42.0, and 87.0 kOe in $CrSiTe_3$ and (c) at 6.0, 42.0, and 87.0 kOe in $CrGeTe_3$. (e) Calculated spin pumping and (f) magnetization for $CrSiTe_3$ at 15.0, 42.0, and 87.0 kOe using the Hamiltonian in Ref. [22].

physics of interface spin pumping from the bulk spin transport [compare Figs. 5(a) and 5(b)]. Here, the interface spin pumping refers to the injection of spin currents by magnetization dynamics at the interface, and should thus be distinct from the bulk spin transport. This decoupling has been shown on picosecond timescales in extreme non-equilibrium using THz pulses [35]. But we demonstrate this in a conventional LSSE experiment in a non-equilibrium but steady-state.

In the ferromagnetic phase below T_C, the LSSE can be understood in the same manner as conventional 3D ferromagnets, such as YIG [33, 34]; in the long-range ordered state, the out-of-plane exchange coupling [17, 22] facilitates the spin transport along the c-axis

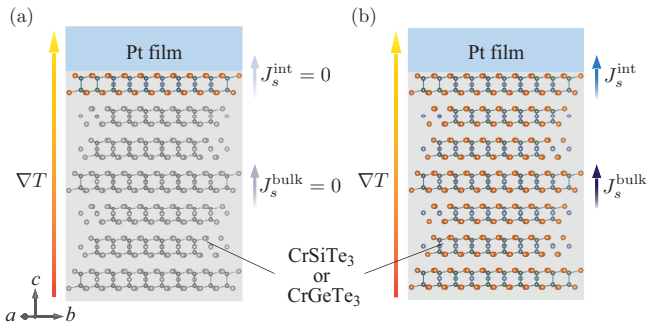

FIG. 5: Schematic illustrations of Pt/$CrSiTe_3$ or Pt/$CrGeTe_3$ under ∇T. (a) For $T \gg T_C$, interfacial spin pumping from the in-plane spin correlations in $CrSiTe_3$ and $CrGeTe_3$ adjacent to the Pt interface is absent ($J_s^{\rm int} = 0$), where bulk spin transport ($\parallel \nabla T$) in $CrSiTe_3$ and $CrGeTe_3$ is inert ($J_s^{\rm bulk} = 0$) since thermal fluctuations mask weak out-of-plane spin exchange interaction J_c at such high temperatures. (b) For $T \leqq T_C$ and the paramagnetic phase just above T_C, bulk spin transport between the planes becomes active ($J_s^{\rm bulk} \neq 0$) and creates non-equilibrium magnon population at the interface, causing finite interfacial spin pumping $J_s^{\rm int}$.

($\parallel \nabla T$) [Fig. 5(b)]. In the paramagnetic phase above T_C, there is no magnetization (in zero magnetic field) and magnons cease to exist. Spin-current transport is therefore not usually observed [36]. In the case of $CrSiTe_3$ and $CrGeTe_3$ however, strong short-range ferromagnetic correlations [17, 22] above T_C form in the ab plane. These spin correlations can be conveyed along the c direction [Fig. 5(b)] via spin-exchange coupling (J_c [17, 22]) [37, 38] and dipole-dipole interactions [39], giving a finite inverse spin-Hall voltage when a moderate H is applied to align spins. Since the LSSE response is observed in a limited T range above T_C [Figs. 4(a) and 4(c)], the exchange coupling is likely to be the primary interaction mediating the interlayer spin transport.

We also examined the T dependence of the LSSE response with high magnetic fields up to 87.0 kOe in Figs. 4(a) and 4(c) (see orange and red dots). As H increases S also increases in magnitude and survives to higher temperatures. For $CrSiTe_3$/Pt [Fig. 4(a)] the S signal at 87.0 kOe appears even at $\sim$ 80 K—more than twice the critical temperature $T_C \sim 31.3$ K

[40]. Under strong magnetic fields, the spin polarization is further enhanced by the Zeeman interaction, which may be responsible for the S increase. This breaks the symmetry of the Hamiltonian so the system no longer exhibits true critical behaviour [41]. This is seen in the M-T curves shown in Figs. 4(b) and 4(d) where the ferro-paramagnetic transition becomes less defined and there is a significant magnetization above the true critical temperature. S decreases more rapidly than M with increasing T [Figs. 4(a) and 4(c)]. The spin Seebeck signal has almost disappeared even though $M > 0.5\ \mu_{\mathrm{B}}$ which also points to the importance of the out-of-plane spin transport in the LSSE. The coupling between the layers (J_c) is insensitive to magnetic fields so the decay rate of S is not relational as with applied fields. Hence S does not show the dependence on M that would be expected for a '3D' magnetic system.

To confirm the above scenario and separate the spin pumping and spin transport of the LSSE we performed atomistic spin dynamics calculations of the (in-plane) magnetization and spin pumping (in the absence of spin transport) [44]. This provides the pure spin pumping contribution of the LSSE without concerns about the magnon distribution at the interface (Its formulation is given by Eq. (6) in Ref. [4]). The Hamiltonian is based on the magnetic parameters of $CrSiTe_3$ reported in Ref. [22]. Our calculations show a good agreement with the M-T curves of the experiments [Figs. 4(b) and 4(d)], although with a slightly higher critical temperature. Figure 4(e) shows T dependence of the spin pumping amplitude at 15, 42 and 87 kOe. Large H increases the spin pumping significantly at temperatures far above T_{C} due to the Zeeman effect; it shows a maximum at approximately 70 K and decreases gently. At 100 K there is still a large difference between the different field values, roughly

proportional to M. This is also consistent with analytic approaches in paramagnets [43]. The reason this is not seen in our experimental measurements is because the out-of-plane spin transport between the layers has vanished and so the magnon distribution at the interface is close to equilibrium. Therefore the paramagnetic spin pumping would not be observed.

To summarize, we studied the LSSE in ferromagnetic transition-metal trichalcogenides $CrSiTe_3$ and $CrGeTe_3$ with Pt contact. In contrast to typical LSSE magnet YIG, the LSSE signal in the $CrSiTe_3$/Pt and $CrGeTe_3$/Pt was found to persist even above T_C. The LSSE above T_C is dominated by thermal spin transport via out-of-plane exchange coupling between the 2D layers. At low magnetic fields the strong short-range ferromagnetic correlations inherent in $CrSiTe_3$ and $CrGeTe_3$ are the main spin current carriers, while the Zeeman energy—comparable in strength to the exchange-coupling—is dominant for the spin alignment under high magnetic fields. Our numerical simulation corroborates the strong magnetic-field effects and points the importance of the interlayer spin transport regardless of the quasi-2D structure. The measurable spin transport across the ferromagnetic Cr layers in $CrSiTe_3$ and $CrGeTe_3$ could be useful in studying spin transports in hetero-structures fabricated with other 2D materials and topological insulators.

The authors thank K. Ohgushi, K. Emi, K. Tanigaki, T. Ogasawara, K. Nawa, and M.Takahashi for their valuable comments on crystal growth. This work was supported by JST ERATO "Spin Quantum Rectification Project" (No. JPMJER1402), JSPS KAKENHI (Nos. JP26103005, JP19H02424, JP19K21039, JP18H04215, JP18H04311, JP19K21031, and JP17K14102), and GP-Spin, Tohoku University. J.B. acknowledges support from the Royal Society through a University Research Fellowship.

* Electronic address: nao.ito@cmpt.phys.tohoku.ac.jp

† Present address: Institute for Molecular Science, Okazaki, Aichi 444-8585 Japan.

[1] K. Uchida, H. Adachi, T. Ota, H. Nakayama, S. Maekawa, and E. Saitoh, Observation of longitudinal spin-Seebeck effect in magnetic insulators, Appl. Phys. Lett. **97**, 172505 (2010).

[2] A. Kirihara, K. Uchida, Y. Kajiwara, M. Ishida, Y. Nakamura, T. Manako, E. Saitoh, and S. Yorozu, Spin-currnt-driven thermoelectric coating, Nat. Mater. **11** 686 (2012).

[3] K. Uchida, M. Ishida, T. Kikkawa, A. Kirihara, T. Murakami, and E. Saitoh, Longitudinal spin Seebeck effect: from fundamentals to applications, J. Phys.: Condens. Mater **26**, 343202 (2014).

[4] J. Barker and G. E. W. Bauer, Thermal Spin Dynamics of Yttrium Iron Garnet, Phys. Rev. Lett. **117**, 217201 (2016).

[5] J. Xiao, G. E. W. Bauer, K. Uchida, E. Saitoh, and S. Maekawa, Theory of magnon-driven spin Seebeck effect, Phys. Rev. B **81**, 214418 (2010).

[6] H. Adachi, J. Ohe, S. Takahashi, and S. Maekawa, Phys. Rev. B **83**, 094410 (2011).

[7] S. Geprägs, A. Kehlberger, F. D. Coletta, Z. Qiu, E.-J. Guo, T. Schulz, C. Mix, S. Meyer, A. Kamra, M. Althammer, H. Huebl, G. Jakob, Y. Ohnuma, H. Adachi, J. Barker, S. Maekawa, G. E. W. Bauer, E. Saitoh, R. Gross, S. T. B. Goennenwein, and M. Kläui, Origin of the spin Seebeck effect in compensated ferrimagnets ,Nat. Commun. **7**, 10452 (2016).

[8] S. Seki, T. Ideue, M. Kubota, Y. Kozuka, R. Takagi, M. Nakamura, Y. Kaneko, M. Kawasaki, and Y. Tokura, Thermal Generation of Spin Current in an Antiferromagnet, Phys. Rev. Lett. **115**, 266601 (2015).

[9] Y. Shiomi, R. Takashima, D. Okuyama, G. Gitgeatpong, P. Piyawongwatthana, K. Matan, T. J. Sato, and E. Saitoh, Spin Seebeck effect in the polar antiferromagnet α-$Cu_2V_2O_7$, Phys. Rev. B **96**, 180414(R) (2017).

[10] S. M. Wu, W. Zhang, A. KC, P. Borisov, J. E. Pearson, J. S. Jiang, D. Lederman, A. Hoffmann, and A. Bhattacharya, Antiferromagnetic Spin Seebeck Effect, Phys. Rev. Lett. **114**, 186602 (2015).

[11] J. Li, Z. Shi, V. H. Ortiz, M. Aldosary, C. Chen, V. Aji, P. Wei, and J. Shi, Spin Seebeck Effect from Antiferromagnetic Magnons and Critical Spin Fluctuations in Epitaxial FeF_2

Films, Phys. Rev. Lett. **122**, 217204 (2019).

[12] S. M. Wu, J. E. Pearson, and A. Bhattacharya, Paramagnetic Spin Seebeck Effect, Phys. Rev. Lett. **114**, 186602 (2015).

[13] C. Liu, S. M. Wu, J. E. Pearson, J. S. Jiang, N. d' Ambrumenil, and A. Bhattacharya, Probing short-range magnetic order in a geometrically frustrated magnet by means of the spin Seebeck effect, Phys. Rev. B **98**, 060415(R) (2018).

[14] B. Shabbir, M. Nadeem, Z. Dai, M. S. Fuhrer, Q. Xue, X. Wang, and Q. Bao, Long range intrinsic ferromagnetism in two dimensional materials and dissipationless future technologies, Appl. Phys. Rev. **5**, 041105 (2018).

[15] S. Lebégue, T. Björkman, M. Klintenberg, R. Nieminen, and O. Eriksson, Two-dimensional Materials from Data Filtering and Ab Initio Calculations, Phys. Rev. X **3**, 031002 (2013).

[16] X. Li and J. Yang, Ultrathin nanosheets of $CrSiTe_3$: a semiconducting two-dimensional ferromagnetic material, J. Mater. Chem. C **2**, 7071 (2014).

[17] C. Gong, L. Li, Z. Li, H. Ji, A. Stern, Y. Xia, T. Cao, W. Bao, C. Wang, Y. Wang, Z. Q. Qiu, R. J. Cava, S. G. Louie, J. Xia and X. Zhang, Discovery of intrinsic ferromagnetism in two-dimensional van der Waals crystals, Nature (London) **546**, 265 (2017).

[18] H. Ji, R. A. Stokes, L. D. Alegria, E. C. Blomberg, M. A. Tanatar, A.Reijnders, L. M. Schoop, T. Liang, R. Prozorov, K. S. Burch, N. P. Ong, J. R. Petta, and R. J. Cava, A ferromagnetic insulating substrate for the epitaxial growth of topological insulators, J. Appl. Phys. **114**, 114907 (2013).

[19] G. Ouvrard, E. Sandre, and R. Brec, Synthesis and Crystal Structure of a New Layered Phase: The Chromium Hexatellurosilicate $Cr_2Si_2Te_6$, J. Solid State Chem. **73**, 27 (1988).

[20] R. E. Marsh, The Crystal Structure of $Cr_2Si_2Te_6$: Corrigendum, J. Solid State Chem. **73**, 190 (1988).

[21] V. Carteauxts, D. Brunet, G. Ouvrardt, and G. Andrdt, magnetic and electronic structures of a new layered ferromagnetic compound $Cr_2Ge_2Te_6$, J. Phys.: Condensed Mater **7**, 69 (1995).

[22] T. J. Williams, A. A. Aczel, M. D. Lumsden, S. E. Nagler, and M. B. Stone, Magnetic correlations in the quasi-two-dimensional semiconducting ferromagnet $CrSiTe_3$, Phys. Rev. B **92**, 144404 (2015).

[23] L. D. Casto, A. J. Clune, M. O. Yokosuk, J. L. Musfeldt, T. J. Williams, H. L. Zhuang, M.-W. Lin, K. Xiao, R. G. Hennig, B. C. Sales, J.-Q. Yan, and D. Mandrus, Strong spin-lattice

coupling in $CrSiTe_3$, APL Mat. **3**, 041515 (2015).

[24] L. D. Alegria, H. Ji, N. Yao, J. J. Clarke, R. J. Cava, and J. R. Petta, Large anomalous Hall effect in ferromagnetic insulator-topological insulator heterostructures, Appl. Phys. Lett. **105**, 053512 (2014).

[25] V. Carteaux, F. Moussa, and M. Spiesser, 2D Ising-like Ferromagnetic Behaviour for the Lamellar $Cr_2Si_2Te_6$ Compound: a Neutron Scattering Investigation, Europhys. Lett. **29**, 251 (1995).

[26] Y. Liu and C. Petrovic, Critical behavior of quasi-two-dimensional semiconducting ferromagnet $CrGeTe_3$, Phys. Rev. B **96**, 054406 (2017).

[27] T. Kikkawa, K. Uchida, S. Daimon, Y. Shiomi, H. Adachi, Z. Qiu, D. Hou, X.-F. Jin, S. Maekawa, and E. Saitoh, Separation of longitudinal spin Seebeck effect from anomalous Nernst effect: Determination of origin of transverse thermoelectric voltage in metal/insulator junctions Phys. Rev. B **88**, 214403 (2013).

[28] B. Liu, Y. Zou, L. Zhang, S. Zhou, Z. Wang, W. Wang, Z. Qu, and Y. Zhang, Critical behavior of the quasi-two-dimensional Semiconducting ferromagnet $CrSiTe_3$, Sci. Rep. **6**, 33873 (2016).

[29] A. K. Pramanik and A. Baneerjee, Critical behavior at paramagnetic to ferromagnetic phase transition in $Pr_{0.5}Sr_{0.5}MnO_3$: A bulk magnetization study, Phys. Rev. B **79**, 214426 (2009).

[30] K. Uchida, T. Kikkawa, A. Miura, J. Shiomi, and E. Saitoh, Quantitative Temperature Dependence of Longitudinal Spin Seebeck Effect at High Temperatures, Phys. Rev. X **4**, 041023 (2014).

[31] T. Kikkawa, K. Uchida, S. Daimon, Z. Qiu, Y. Shiomi, and E. Saitoh, Critical suppression of spin Seebeck effect by magnetic fields, Phys. Rev. B **92**, 064413 (2015).

[32] H. Jin, S. R. Boona, Z. Yang, R. C. Myers, and J. P. Heremans, Effect of the magnon dispersion on the longitudinal spin Seebeck effect in yttrium iron garnets, Phys. Rev. B **92**, 054436 (2015).

[33] S. M. Rezende, R. L. Rodríguez-Suárez, R. O. Cunha, A. R. Rodrigues, F. L. A. Machado, G. A. Fonseca Guerra, J. C. Lopez Ortiz, and A. Azevedo, Magnon spin-current theory for the longitudinal spin-Seebeck effect, Phys. Rev. B **89**, 014416 (2014).

[34] L. J. Cornelissen, K. J. H. Peters, G. E. W. Bauer, R. A. Duine, and B. J. van Wees, Magnon spin transport driven by the magnon chemical potential in a magnetic insulator, Phys. Rev. B **94**, 014412 (2016).

[35] T. S. Seifert, S. Jaiswal, J. Barker, S. T. Weber, I. Razdolski, J. Cramer, O. Gueckstock, S. F. Maehrlein, L. Nadvornik, S. Watanabe, C. Ciccarelli, A. Melnikov, G. Jakob, M. Münzenberg, S. T. B. Goennenwein, G. Woltersdorf, B. Rethfeld, P. W. Brouwer, M. Wolf, M. Kläui, and T. Kampfrath, Femtosecond formation dynamics of the spin Seebeck effect revealed by terahertz spectroscopy, Nat. Commun. **9**, 2899 (2018).

[36] Y. Shiomi and E. Saitoh, Paramagnetic Spin Pumping, Phys. Rev. Lett. **113**, 266602 (2014).

[37] H. S. Bennett and P. C. Martin, Spin Diffusion in the Heisenberg Paramagnet, Phys. Rev. **138**, A608 (1965).

[38] D. Wesenberg, T. Liu, D. Balzar, M. Wu, and B. L. Zink, Long-distance spin transport in a disordered magnetic insulator, Nat. Phys. **13**, 987 (2017).

[39] K. Oyanagi, S. Takahashi, L. J. Cornelissen, J. Shan, S. Daimon, T. Kikkawa, G. E. W. Bauer, B. J. van Wees, and E. Saitoh, Efficient spin transport in a paramagnetic insulator, arXiv:1811.11972 (2018).

[40] S curves become linear with respect to H above 65 K for the $CrSiTe_3$/Pt and 85 K for $CrGeTe_3$/Pt [see the $S(H)$ result at 100 K shown in Figs. 3(a) and 3(c)]. Above these temperatures, we cannot distinguish the contribution from a H-linear normal Nernst effect to the S signal [27]. We thus avoid a detailed discussion on the high-H-induced S enhancement above 65 K for $CrSiTe_3$/Pt and above 85 K for $CrGeTe_3$/Pt.

[41] N. Goldenfeld, Chapter 9: The Renormalisation Group, in *Lectures on Phase Transitions and the Renormalization Group* (Perseus Books, Reading, Massachusetts, 1992).

[42] J. Barker, and G. E. W. Bauer, Quantum thermodynamics of complex ferrimagnets, arXiv:1902.00449 (2019)

[43] S. Okamoto, Spin injection and spin transport in paramagnetic insulators, Phys. Rev. B **93**, 064421 (2016).

[44] Using the same methodology as Ref. [4] but with quantum (Planck) statistics for the thermal fields to correctly describe magnons at these low temperatures [42].